Integrative species delimitation in the common ophiuroid *Ophiothrix angulata* (Echinodermata: Ophiuroidea): insights from COI, ITS2, arm coloration, and geometric morphometrics

5 Yoalli Quetzalli Hernández-Díaz[1,2,*], Francisco Solís[2], Rosa Gabriela Beltrán-López[3,4], Hugo A.
6 Benítez[5,6], Píndaro Díaz-Jaimes[7], Gustav Paulay[8]

7 [1]Posgrado en Ciencias del Mar y Limnología, Universidad Nacional Autónoma de México, Av.
8 Universidad 3000, Ciudad Universitaria Coyoacán, C.P. 04510, Ciudad de México, México.

9 [2]Laboratorio de Sistemática y Ecología de Equinodermos, Instituto de Ciencias del Mar y
10 Limnología, Universidad Nacional Autónoma de México, Ciudad de México, México

11 [3]Laboratorio de Ictiología, Centro de Investigaciones Biológicas, Universidad Autónoma del
12 Estado de Morelos, Cuernavaca, México

13 [4]Departamento de Zoología, Instituto de Biología, Universidad Nacional Autónoma de México,
14 Ciudad de México, México

15 [5]Laboratorio de Ecología y Morfometría Evolutiva, Centro de Investigación de Estudios
16 Avanzados del Maule, Instituto Milenio Biodiversidad de Ecosistemas Antárticos y
17 Subantárticos (BASE), Universidad Católica del Maule, Talca 3466706, Chile

18 [6]Centro de Investigación en Recursos Naturales y Sustentabilidad (CIRENYS), Universidad
19 Bernardo O'Higgins, Avenida Viel 1497, Santiago 8370993, Chile

20 [7]Laboratorio de Genética de Organismos Acuáticos, Instituto de Ciencias del Mar y Limnología,
21 Universidad Nacional Autónoma de México, Ciudad de México, México

22 [8]University of Florida, Florida Natural History Museum, Gainesville, USA

23 Corresponding author: *quetzalli.hernandez@ciencias.unam.mx

Abstract

25 *Ophiothrix angulata* (Say, 1825) is one of the most common and well-known ophiuroids in the
26 Western Atlantic, with a wide geographic and bathymetric range. The taxonomy of this species
27 has been controversial for a century because of its high morphological variability. Here we
28 integrate information from DNA sequence data, color patterns, and geometric morphometrics to
29 assess species delimitation and geographic differentiation in *O. angulata*. We found three deeply
30 divergent mtDNA-COI clades (K2P 17.0–27.9%). ITS2 nuclear gene and geometric
31 morphometrics of dorsal and ventral arm plates differentiate one of these lineages, as do
32 integrative species delineation analyses, making this a confirmed candidate species.

33 Keywords: mitochondrial DNA, morphology, geometrics morphometrics, integrative taxonomy,
34 Caribbean, Gulf of Mexico, coral reefs.

Introduction

36 Members of the Class Ophiuroidea, brittle stars, basket stars, and snake stars, are the most
37 diverse of the five echinoderm classes, and are often abundant and, at times, dominant members
38 of marine benthic communities (Kissling & Taylor, 1977; Lewis & Bray, 1983; Hendler &
39 Littman, 1986; Aronson, 1988; Stöhr, O'Hara & Thuy, 2012; Boissin et al., 2016). While the
40 taxonomy of ophiuroids was thought to be well known, sequence data has demonstrated that
41 numerous well-known brittle stars are complexes of cryptic species (e.g. the cosmopolitan
42 *Amphipholis squamata* (Boissin et al., 2008) and the Northeastern Atlantic *Ophiothrix fragilis*
43 (Pérez-Portela, Almada & Turon, 2013; Taboada & Pérez-Portela, 2016).

44 The tropical Western Atlantic (WA) is home to the second major coral reef realm, has very high
45 diversity and endemicity, and hosts a remarkably abundant, rich, and ecologically diverse brittle
46 star fauna (Kissling & Taylor, 1977; Stöhr, O'Hara & Thuy, 2012; Sobha, Vibija & Fahima,
47 2023). The Ophiotrichidae (Ljungman, 1867) is the third-largest family of brittle stars and is
48 well-represented in the WA. Ophiuroids have undergone extensive systematic revision following
49 recent phylogenomic studies, and ophiotrichids were found to be "genetically and
50 morphologically coherent" (O'Hara et al., 2018). Although ophiuroids have become well-defined
51 at the family level, substantial work remains on many genera and species. *Ophiothrix* is the
52 largest brittle star genus with 96 accepted species (dos Santos Alitto et al., 2019; Santana et al.,
53 2020; Stöhr, O'Hara & Thuy, 2023), but neither the genus nor its subgenera are monophyletic
54 (O'Hara et al., 2017; O'Hara et al., 2018). The high diversity and morphological variability of
55 ophiotrichids have made their species-level taxonomy challenging (Clark, 1946; Clark, 1967;
56 Tommasi, 1970; Hoggett, 1991; Hendler, 2005).

57 Traditional species delineation of ophiuroids has focused on macro-morphological characters
58 that can show substantial variability and overlap among species, causing taxonomic confusion
59 (Arlyza et al., 2013). An integrative approach that combines information from live appearance,
60 microstructure, life history, ecology, ethology, physiology, distribution, and especially DNA
61 sequence data provides information to resolve species in challenging groups like *Ophiothrix*
62 (Bickford et al., 2007; Boisson et al., 2008; Padial et al., 2010; Pérez-Portela, Almada & Turon,
63 2013; O'Hara et al., 2014a; Richards, DeBiasse & Shivji, 2015; Taboada & Pérez-Portela, 2016;
64 dos Santos Alitto et al., 2019; Newton et al., 2020). Over the past decade, the use of
65 microstructural characters has emerged as a valuable tool in systematic studies of brittle stars,
66 revealing their phylogenetic value (O'Hara et al., 2014b; Thuy & Stöhr, 2016). Among these
67 characters, arm plates have proven to be particularly important in establishing a congruence with
68 molecular data, enabling the inference of phylogenetic relationships even at the genus level
69 (Thuy & Stöhr, 2016). Therefore, these characters offer a valuable approach to analyze species
70 complexes and contribute to species delimitation.

71 *Ophiothrix angulata* (Say, 1825) was one of the first brittle stars and the first ophiotrichid
72 described for the Americas. It is nearly ubiquitous along the Atlantic coasts of North and South
73 America in warm temperate to tropical waters, from North Carolina, USA to at least Venezuela,
74 and throughout the Caribbean islands, Bahamas, and Bermuda (Devaney, 1974; Herrera-Moreno
75 & Betancourt Fernández, 2004; Alvarado, Solís-Marín, & Ahearn, 2008; Borrero-Pérez et al.,
76 2008; del Valle García et al., 2008; Laguarda-Figueras et al., 2009; Alvarado & Solís-Marín,
77 2013; Noriega & Fuentes-Carrero, 2014; Sandino et al., 2017; 'GBIF.org', 2022). Records of *O.*
78 *angulata* further south are now attributed to other species (Santana et al., 2017; Santana et al.,
79 2020). The species also has a broad bathymetric distribution from intertidal to bathyal depths
80 (~1,000 m; ICML-UNAM 3.34.40: 770 m; MCZ OPH-30910: 1,499 m). This species is capable
81 of inhabiting corals, sponges, being under rocks, and among turf algae, which gives it a great
82 capacity to adapt to different micro-habitats.

83 *Ophiothrix angulata* is highly variable and has a broad latitudinal and bathymetric distribution
84 that has attracted taxonomic attention (Tommasi, 1970; Clark, 1933; Hendler et al., 1995;
85 Hendler et al., 1999; Hendler, 2005; Santana et al., 2017). Variation is especially notable in color
86 (Lyman, 1865; Verrill, 1899; Clark, 1901), and Clark (1918) named five varieties based on this.
87 The species has also been noted to vary in disc shape, and arrangement of spinelets around the
88 disc, but Hendler et al. (1995), concluded that this variation does not seem to sort into species-
89 level units.

90 The goal of this study was to assess whether the great morphological diversity of *O. angulata* is
91 the result of high intra-specific variation or differentiation among multiple cryptic or pseudo-
92 cryptic species. We tested species boundaries using an integrative taxonomic approach, by
93 combining mtDNA COI and nrDNA ITS2 sequence data color patterns, and geometric
94 morphometrics of dorsal and ventral arm plates. We combined results from genetic and
95 morphological assessments for species delimitation using an integrated Bayesian phylogenetics
96 and phylogeography approach (iBPP) (Solís-Lemus, Knowles & Ané, 2015). We also analyzed
97 the population diversity and demographic history of the clades discovered.

Materials & Methods

Sampling sites and collections

100 We used 146 *Ophiothrix angulata* specimens from 24 localities across the West Atlantic (Fig. 1;
101 Table S1). Thirty-five samples were collected specifically for this project; others were obtained
102 from collections at the Invertebrate Zoology Collection, Florida Museum of Natural History,
103 University of Florida (UF); University of West Florida (UWF); Natural History Museum of Los
104 Angeles County (LACM); Colección Nacional de Equinodermos "Dra. María Elena Caso
105 Muñoz", Instituto de Ciencias del Mar y Limnología, UNAM, México (ICML-UNAM);
106 Colección Regional de Equinodermos de la Península de Yucatán, UMDI-Sisal, UNAM, México
107 (COREPY-UNAM). Field sample collection where approved by Secretaría de Agricultura,
108 Ganadería, Desarrollo Rural, Pesca y Alimentación (SAGARPA: Permission number:
109 PPF/DGOPA-082/19), and Museo de Zoología, Escuela de Biología, Universidad de Costa Rica

110   (MZ-UCR). All 146 individuals were sequenced for COI, 14 for ITS, 46 were selected for
111   geometrics morphometric analyses while living color pattern was examined for 46 specimens
112   from the UF and COREPY photographic collections. Twelve additional sequences available
113   from GenBank were also used (Table S1). Nine terminals from five outgroup species were also
114   sequenced: *Ophiothrix cimar* (Hendler, 2005); *Ophiothrix lineata* (Lyman, 1860); *Ophiothrix stri*
115   Hendler, 2005; *Ophiothrix suensoni* (Lütken, 1856) and *Ophiactis savignyi* (Müller & Troschel,
116   1842).

117   **DNA extraction and sequence alignment**
118   DNA was extracted from ethanol-fixed arm tissue using the Chelex protocol (Walsh, Metzger &
119   Higuchi, 1991) or the Omega Bio-Tek E.Z.N.A. Mollusc DNA kit according to the
120   manufacturer's instructions. The echinoderm barcoding primers COIceF and COIceR (Hoareau
121   & Boissin, 2010) were used to amplify a 655-base pair (bp) region of COI as described by
122   Michonneau & Paulay (2014). Electropherograms were checked, assembled into contigs, and
123   manually edited using Sequencher 4.6 (Gene Code Corps, Ann Arbor, Michigan). Consensus
124   sequences were aligned using Muscle (Edgar, 2004), and alignment was verified by eye using
125   PhyDE v.10.0 (Müller et al., 2010). The sequence alignment was converted to protein using
126   Genius v8.1.7 (Kearse et al., 2012) to ensure a proper reading frame and to verify the absence of
127   stop codons. A 527 pb section of the nuclear DNA internal transcribed spacer-2 (ITS-2) was
128   amplified using the primers OphITS2F and OphITS2R as described by Naughton et al. (2014).
129   Sequences were deposited in GenBank (COI accession numbers: MT338285–MT338398,
130   ON245084–ON245096; ITS accession numbers: OQ225473–OQ225482).

131   **Phylogenetic analyses**
132   Phylogenetic analyses using Bayesian Inference (BI) and Maximum Likelihood (ML) methods
133   were performed separately for COI and ITS2 sequence datasets on the CIPRES Science Gateway
134   portal (Miller, Pfeiffer & Schwartz, 2010). jModelTest2 (Darriba et al., 2012) was used on the
135   CIPRES portal to select the best model of molecular evolution based on Akaike information
136   criteria tests (AIC). ML analyses were done using RAxML-HPC2 on XSEDE (Stamatakis, 2006;
137   Stamatakis, Hoover & Rougemont, 2008) with the GTR+GAMMA model of sequence evolution;
138   nodal support values were assessed with 1,000 rapid bootstraps (Felsenstein, 1985). BI analyses
139   were performed using MrBayes v.3.2.7a on XSEDE (Ronquist et al., 2012), using the GTR+I+G
140   model. The MCMC search was based on two independent runs of four chains each and 6,000,000
141   generations (sampled every 1,000 generations) until the final average and standard deviation
142   were close to 0.01. Twenty-five percent of the initial trees were discarded as Burn-in. Results
143   were summarized in Tracer v.1.7.1 (Rambaut et al., 2018) based on the Effective Sample Size-
144   ESS for each parameter. The gene phylogenies were represented using FigTree v.1.4.4
145   (Rambaut, 2018) and annotated using Adobe Illustrator CC v.2017-22.0.1.

146   **Geometric morphometric analyses**
147   We analyzed dorsal arm plates (DAP) and ventral arm plates (VAP) from 46 specimens. Images
148   of DAP and VAP were taken through scanning electron microscopy (SEM) from intermediate-

149   sized specimens with disc diameters (DD) of 2.5 to 5.5 mm to assess the size-independent
150   variability. The integument was removed from the 4th–8th arm segments (counted from the first
151   arm segment that contained a regular vertebra and lateral plates (Stöhr, 2005)), due to the adult
152   proximal arm plates have shown the highest degree of morphological differentiation, reflecting
153   differences between species (Thuy & Stöhr, 2011). The integument removal was performed by
154   submergence in 0.3% sodium hypochlorite solution for 2–8 hours, washed with distilled water
155   and 98% ethanol, air-dried, and mounted on aluminum stubs using carbon tape. The samples
156   were then gold-coated and scanned using a Hitachi-SU1510 SEM at the LANABIO facility at the
157   Instituto de Biología, UNAM.

158   In order to organize the data for analyses, the file format of the plate images was imported into
159   TPS file format using tpsUtil v.1.58. Landmarks and curves were digitized using tpsDig2 v.2.17
160   (Rohlf, 2013). Along the external margin of each DAP, five homologous type II landmarks and
161   sixty-eight evenly-spaced semi-landmarks were digitized (Fig. 2A). The same procedure was
162   followed for VAP but using four landmarks type II and 66 semi-landmarks evenly-spaced (Fig.
163   2B). Geometric Morphometric (GM) analyses followed the outlined by Masonick & Weirauch
164   (2019), using the R package *geomorph* v.3.2.1 R package (Adams & Otárola-Castillo, 2013).
165   The GM analyses compared four clades and subclades defined by COI sequence data set (Table
166   S2): Clade 1A, Clade 1B, Clade 2A, and Clade 3. Generalized Procrustes analysis was used to
167   extract the shape data for comparison, removal, translation, scaling, and rotation of all selected
168   landmarks. A proxy of size in GM is centroid size which is the square root of the sum of squared
169   distances of an object's landmarks from their centroid or center of gravity.

170   The semi-landmarks digitized for each arm plate were optimized to reduce bending energy using
171   the function ProcD=False in *geomorph*, thus providing the best fit during optimization. Shape
172   variation was analyzed through Principal Component Analysis (PCA) using the covariance
173   matrix of the individual, and a graphical scatterplot was performed using the two principal
174   components, which accumulated the maximum variance of the data (PC1 vs. PC2; S3 Appendix).
175   Thin-plate spline deformation grids were calculated from the mean shape variance along each PC
176   axis with the *shapes* v.1.2.5 R package (Dryden, 2018), representing the overall shape
177   modification. To enhance the visualization of data dispersion, two scatterplots in 3D were
178   constructed based on the first three PCs using the R package *car* v.3.0-6 (Fox, Weisberg & Price,
179   2018; Masonick & Weirauch, 2019). A Procrustes analysis of variance (ANOVA) was
180   performed on all analyses using the "procD.lm" function in *geomorph*. The resulting pairwise
181   Procrustes distances were compared to assess the significance of differences in mean arm plate
182   shape among the groups. The significance of the observed variation was assessed through a
183   permutation test of the randomized model residuals with 999 iterations at an α-value of 0.05.

184   **Measurement Error and Allometry-test**
185   To evaluate the impact of measurement error, the selected landmarks were digitized twice on
186   each image (dorsal and ventral arm plates), on different days, by the same observer (Viscosi &
187   Cardini, 2011). The error was calculated as percent measurement error (%ME) by comparing the

188   variation among measurements based on a formula developed by (Bailey & Byrnes, 1990;
189   Yezerinac, Lougheed, & Handford, 1992). A Procrustes ANOVA on the residuals of Procrustes
190   distances was used to compare within and among individual shape variance components. The
191   allometry was evaluated by regression of the Procrustes shape coordinates on centroid size using
192   a $\log_{10}$ scale. Interaction between Centroid size and "clade" (dorsal or ventral arm plates grouped
193   by clade) factor was estimated with Procrustes ANOVA in *geomorph* v.3.2.1 (Klingenberg,
194   2016).

Dorsal arm color pattern analysis

195
196   Color patterns were examined from live-taken images associated with 46 sequenced specimens
197   from the UF and COREPY invertebrate image collections (Table S1). Twenty-five color
198   characters were selected from dorsal arm views (Figs. S1, S2, and S3). All characters were
199   treated as discrete and unordered (S1 Appendix). Disc color characters were not selected because
200   they showed a great amount of individual variation. *Ophiactis savignyi* was used as outgroup
201   species (Fig. S4).

202   The character matrix was edited in Mesquite v.3.51 (Maddison & Maddison, 2018), with
203   inapplicable data scored with "-" (S2 Appendix). Parsimony analysis was conducted using TNT
204   v.1.5 (Goloboff & Catalano, 2016). Optimal trees were searched using random addition
205   sequences of Wagner trees, followed by the TBR algorithm, using 500 replicates, and saving 10
206   trees per replicate. The resulting trees were used as starting points for a round of TBR branch
207   swapping. Bootstrap support values for the strict consensus tree were determined through 1000
208   iterations, with default settings. Visualization, interpretation, and annotation of the cladogram
209   were performed with FigTree, TNT, and Illustrator, respectively.

Molecular species delimitation

210
211   Two sequence-based species delimitation methods were employed using mtDNA data only.
212   Multi-rate Poisson tree processes (mPTP) is a non-coalescent, sequence-based, maximum
213   likelihood method that does not require pre-determined taxonomic designations and uses
214   statistical cutoffs to delineate taxa on a phylogenetic input tree (Zhang et al., 2013; Kapli et al.,
215   2017). It identifies variation in the pace of branching events, modeling speciation based on the
216   number of substitutions. The online version of mPTP (https://mptp.h-its.org/#/tree) was used to
217   calculate species delimitation, using the Bayesian tree as input, mPTP model selected, with nine
218   specimens as outgroup taxa. The resulting trees were visualized using FigTree v.1.4.4.

219   Bayesian program BPP v.4.1.4 (Yang, 2015) to infer phylogenetic and phylogeographic patterns
220   under the multispecies coalescent model (MSC) was used to calculate potential species' posterior
221   probabilities delimitation (Yang & Rannala, 2010; Yang, 2015). BPP appears to be relatively
222   robust to the influence of unequal population sizes, rates of population growth, unbalanced
223   sampling, and mutation rate heterogeneity (Luo et al., 2018), and has proven effective in
224   analyses of taxon evolution and divergence (Zhang et al., 2013; Moritz et al., 2018). A 151-taxon
225   dataset and the Bayesian tree were used for all BPP analyses, because sequences with missing

226   data were eliminated. The estimation of appropriate starting species divergence times (τs) and
227   population size parameters (θs) was initially performed through A00 BPP analysis (Masonick &
228   Weirauch, 2019). This estimation was based on the expected number of mutations per kilobase,
229   as Yang (2015) described. The parameters for the MSC model were estimated using BPP v4.1.4
230   (following the A00 analysis from Yang, 2015). The joint species tree estimation and species
231   delimitation analyses (A11) were carried out with inverse-gamma parameters of θ (5, 0.05) and τ
232   (5, 0.02). The A11 analysis was run for 100,000 generations, sampling every two steps after
233   discarding the initial 10,000 generations as burn-in. The analysis results were confirmed by
234   conducting three independent runs for each analysis. Only lineages with a posterior probability
235   (pp) of ≥ 0.95 were considered well-supported (Masonick & Weirauch, 2019).

Integrative species delimitation

237   Morphological and mtDNA were analyzed in a common coalescent Bayesian framework using
238   the program iBPP v.2.1.3 (Solís-Lemus, Knowles & Ané, 2015). This method has been shown to
239   improve species delimitation accuracy by incorporating molecular and quantitative phenotypic
240   data in the assessment of *a priori* species assignments using a guide tree. iBPP analyses were
241   performed using the Bayesian topology as a guide tree. The same values for demographic
242   parameters θ and τ as in the BPP analysis were used. The total evidence analyses described
243   below utilized two datasets, as iBPP is capable of incorporating morphological data represented
244   by quantitative, continuous traits: a) multistate character matrix with the 25 arm color-characters
245   as trait data scored through the color pattern analysis, and b) PC1 + PC2 values for DAP and
246   VAP as trait data obtained through the GM analysis. For both analyses, 46 specimens were used
247   that included sequences and GM data, and the second included the specimens with sequences
248   and the photographic record *in vivo*. To determine if different data types result in congruent
249   delimitations, the following comparisons were made among data types: sequence data only,
250   coloration data only, GM data only, sequence and coloration data (iBPP$_{Seq+COL}$), and sequence
251   and GM data (iBPP$_{Seq+GM}$) (Masonick & Weirauch, 2019). Posterior probabilities (pp) at each
252   node were averaged after performing each analysis three times. After a burn-in phase of 10,000
253   iterations, every second tree was sampled for a total of 100,000 trees. Well-supported
254   delimitations were only considered for nodes on the guide tree that were recovered with pp
255   values of ≥ 0.95 (Masonick & Weirauch, 2019).

Population diversity

257   Standard measures of genetic diversity (number of haplotypes, haplotype diversity h, and
258   nucleotide diversity π) were calculated using Arlequin v.3.5.2.2 (Excoffier & Lischer, 2010).
259   Unique haplotypes were identified using DnaSP v6.12 (Rozas et al., 2017). Geographical
260   relationships of mtDNA haplotypes were summarized using the TCS algorithm (Clement et al.,
261   2002) in the software PopART v.1.7 (Leigh & Bryant, 2015). To perform the homologous
262   character comparison, missing data were excluded by trimming sequences to 632bp. For
263   comparison with other ophiuroid species, evolutionary distance values were generated in MEGA
264   11 (Tamura, Stecher & Kumar, 2021) using the Kimura 2-parameter model (Kimura, 1980),

265 support values based on 1,000 bootstraps, including both transitions and transversions, the rate
266 variation among sites was modeled with a gamma distribution (shape parameter = 1), codon
267 positions included were $1^{st} + 2^{nd} + 3^{rd}$, and missing data were treated as pairwise deletion (Table
268 1).

269 **Demographic history**
270 To test for past population expansions, Fu's *Fs* test (Fu, 1997) was implemented in Arlequin
271 v.3.5.2.2, and significance was assessed with 1,000 permutations. In addition, values of
272 mismatch frequency were obtained in Arlequin and plotted with the R package *ggplot2*
273 (Wickham, 2016) to determine whether the populations exhibit evidence of spatial/demographic
274 expansions or a stationary population history (Tajima, 1989). The Raggedness index and the sum
275 of squared deviations (SSD) obtained in Arlequin were used to analyze the goodness of fit for the
276 population expansion model, according to Harpending (1994).

277 ## Results

278 **Genetic differentiation and spatial distribution**
279 The consensus COI phylogenetic trees showed three deeply divergent (K2P distances 17.0–
280 27.9%; Table 1), highly supported (PP/bootstrap at 100/ ≥ 90) clades in *Ophiothrix angulata*
281 with both methods (BI and ML) (Fig. 3). Two clades (Clade 2 and Clade 3) are widespread,
282 whereas Clade 1 has a more restricted range (Fig. 1). The three clades have overlapping depth
283 ranges down to 45 m, with only Clade 3 extending deeper, with five sequenced specimens from
284 45–135 m (Fig. S5). COI haplotype networks recovered the same groups obtained in the
285 phylogenetic tree. Haplogroup 1 (Clade 1) was separated from Haplogroup 2 (Clade 2) by 64
286 mutational steps (m-s), while Haplogroup (Clade 3) was separated by 110 m-s from Clade 1, and
287 by 96 m-s from Clade 2. Clades 1 and 2 were not differentiated in ITS2, but Clade 3 was
288 divergent (Fig. 4).

289 **Clade 1**
290 Clade 1 (n=76) was encountered only in the Gulf of Mexico and east Florida, including the
291 Veracruz platform reefs in the Southern Gulf of Mexico and Northern Gulf of Mexico at 0–41 m
292 depths (Fig. S5). Although it overlaps in distribution and depth with clades 2 and 3, the latter are
293 widely distributed across the sampled areas (Fig. 1). Three sympatric subclades can be
294 differentiated within Clade 1 (Figs. 3 and 5), that cooccur in the Northern Gulf of Mexico and
295 the Florida Keys.

296 **Clade 2**
297 Clade 2 (n=51) was collected in almost all areas sampled (Northern Gulf of Mexico, Florida
298 Keys, East Florida, Southern Gulf of Mexico, Western Caribbean, Southwestern Caribbean, and
299 the Eastern Caribbean; Fig. 1) at 0.5–42 m depths (Fig. S5). Two deeply divergent (5.1% K2P),
300 allopatric subclades can be differentiated in Clade 2: a widely distributed subclade 2A (n=49)
301 that displays a star-like haplotype network (Fig. 5), and subclade 2B (n=2) sampled only in
302 Guadeloupe (Eastern Caribbean).

Clade 3

Clade 3 included 31 specimens from Northwest Florida, Florida Keys, Campeche Bank, Western Caribbean, and Eastern Caribbean (Fig. 1) at 1.5–135 m depths (Fig. S5). This clade shows high levels of differentiation, with almost all specimens having distinct COI sequences, separated by multiple substitutions up to ~5.3% K2P (Fig. 6).

Geometric morphometrics

Procrustes ANOVA showed significant differentiation among clades for DAP and VAP (p-value <0.05). Clades 1A, 1B, and 2A clustered together, while Clade 3 separated in the morpho-space and was significantly different based on pairwise comparisons among clades for both arm plates (Table S3). Corresponding thin-plate spline (TPS) deformation grids for PC1 in DAP analysis illustrate the extremes of variation with the extension/shortening of proximal and lateral edges, while PC2 shows the extension/shortening of the distal edge (Fig. 7). TPS deformation grids in VAP indicate that a considerable portion of the variance in PC1 is attributed to the extension/shortening of both, the proximal and distal edges, as well as and the lateral edges. In contrast, PC2 shows the extension/shortening of proximal and distal edges (Fig. 8). To further illustrate how clades groups in morpho-space, three-dimensional scatterplots of the three principal components (PCs) for both DAP and VAP analyses are provided (Figs. S6 and S7). Delimitations based on significantly different DAP and VAP shapes tested in GM analysis are shown in Figs. 7 and 8, respectively; the DAP and VAP analysis results show a correlation with molecular evidence supporting the three clades' relationship. The Multivariate Regression showed that 16.7% of the variation for DAP and 9.0% for VAP was attributable to allometric variation in shape; this variation showed no significant interaction for any plate between Centroid size and "clade" factor in Procrustes ANOVA (p-value > 0.05). Measurement errors were low, 1.53% for DAP and 3.05% for VAP.

Dorsal arm color pattern analysis

All but four (characters 16, 19, 22, and 25) of the 25 selected color-characters were parsimony informative, but none showed concordant differences with genetic clade assignment (Fig. S8). The consensus tree length was 170 steps, with CI=0.201 and RI=0.479. Specimens from all clades clustered together.

Molecular species delimitation

BPP analyses recovered Clades 1, 3, and subclades 2A, and 2B as distinct, with posterior probability values of >99 for all clades. mPTP species delimitations recovered the same clades as BPP (Fig. 9).

Integrative species delimitation.

iBPP analyses recovered Clades 1A, 1B, 2, and 3 as distinct for both iBPP$_{Seq+GM}$ and iBPP$_{Seq}$, with high support in all runs. iBPP$_{GM}$ separated Clade 3 with high support, but low support was found between clades 1A, 1B, and 2. iBPP$_{Seq+COL}$ and iBPP$_{COL}$ did not show congruence in runs, so all clade specimens clustered together (Fig. S9).

341 **Population diversity**
342 Haplotype diversity (h) and nucleotide diversity (π) ranged from 0.743 to 1.000 and from 0.007
343 to 0.048, respectively, among the clades (Table 2). TCS network recovered the same three clades
344 as the phylogenetic analysis of mtDNA. Nucleotide (π) and haplotype (h) diversity values in the
345 TCS network indicated that Clade 3 was more genetically diverse, followed by Clade 1, while
346 Clade 2 exhibited lower nucleotide and haplotype diversity (Table 2).

347 **Demographic history**
348 Results of Fu's Fs tests, Raggedness index, and SSD analysis are provided in Table 2. Fu's
349 neutrality test gave significant negative values for all clades, and subclades 1A and 1B**,**
350 suggesting past demographic expansions. The Raggedness index and SSD were low and non-
351 significant for all clades and subclades 1A and 1B, respectively, suggesting an unimodal
352 distribution of mismatches as expected for a demographic expansion. The distribution of
353 mismatches for Clades 1 and 3 was bimodal (Fig. S10), which may indicate demographic
354 balance. However, when clades 1A and 1B were analyzed separately, mismatches showed a
355 unimodal distribution for 1A while continued bimodal for 1B (Fig. S11). The mismatch
356 distribution of Clade 2 was unimodal (Fig. S10).

357 # Discussion
358 **Species delimitation in _Ophiothrix angulata_**
359 Analysis of COI sequence data revealed three deeply-divergent clades within _Ophiothrix_
360 _angulata_ in the tropical Western Atlantic, one of which (Clade 3) was also divergent in ITS2 and
361 geometric morphometrics. Species delineation algorithms recovered the same three clades using
362 genetic and combined genetic and morphometric data. The deep level of genetic differentiation
363 with COI among these clades is also consistent with the three lineages representing separate
364 species (Table 1).

365 The consistency between morphological and genetic data on differentiate Clade 3, together with
366 its co-occurrence with clades 1 and 2, demonstrates the lack of gene flow between Clade 3 and
367 the others, and clearly establishes that it is a separate biological species; thus, it can be
368 considered a confirmed candidate species (CCS) (Padial et al., 2010). All three clades co-occur
369 in the Florida Keys, where they were collected on the same day, site, depth, and habitat
370 (UF10247-1A, UF10248-2A, and UF10250-3 in Table S1), which further suggests reproductive
371 isolation for Clade 3.

372 The status of clades 1 and 2 remain open, as they were separated only by COI sequences, and
373 thus could be species or deep conspecific lineages (DCL) (Padial et al., 2010). While the
374 distribution of these two clades overlaps and they are sympatric at several localities surveyed,
375 Clade 1 is mostly known from around central and North Florida, while Clade 2 was encountered
376 in South Florida, Southern Gulf de Mexico, and the Caribbean. This distribution largely reflects
377 the differentiation of Gatunian and Callosahatchian faunas that have been established since the
378 Miocene (Vermeij, 2005) and suggest allopatric differentiation along this boundary. Additional
379 studies are needed to assess their status.

380 Clustering sequences into three subclades in Clade 1 and two subclades in Clade 2 is more
381 challenging to interpret. In Clade 2, the two subclades are allopatric, with one represented by two
382 specimens from the Lesser Antilles, the other widespread, suggesting geographic differentiation.

383 **Geometric morphometrics and Dorsal arm color pattern**
384 The shape of both the dorsal and ventral arm plates proved to be a useful indicator for
385 distinguishing Clade 3 from Clades 1-2. Geometric morphometrics has been employed in
386 echinoderm studies to investigate different approaches to understanding the biology and
387 classification of the different orders and families. For instance, Martínez-Melo, De Luna &
388 Buitrón-Sánchez (2017) used GM methods to differentiate between genera in the Cassidulidae
389 family based on the cryptic morphology of plate shapes in Echinoidea. De los Palos-Peña et al.
390 (2021), combined scanning electron microscopy and ontogenetic studies of the odontophore in
391 *Luidia superba* to understand patterns of size and shape variation. Similarly, Swisher (2021)
392 studied ontogeny in fossil clypeasteroids and confirmed size and shape changes in the oral/aboral
393 plates using GM methods. However, our study incorporates the concept of allometry, which
394 considers the effect of size on shape variation due to ontogeny and other ecological factors
395 influencing morphology (Benítez et al., 2013; Klingenberg, 2022).

396 Closely related species frequently differ in color pattern and color differences are often among
397 the first visible morphological changes that appear among differentiating species (Benavides-
398 Serrato & O'Hara, 2008; Hoareau et al., 2013). *Ophiothrix angulata* displays high polymorphism
399 in color patterns (Figs. S1, S2, and S3), and color differences have been suggested to potentially
400 reflect cryptic species differentiation in this species (Clark, 1918; Tommasi, 1970). The absence
401 of correlation between color pattern and genetic clade in our study suggests that color variation is
402 an intra-specific trait. This finding is consistent with previous studies on the *Ophiothrix fragilis*
403 complex, a widely distributed species in the Northeastern Atlantic Ocean. Previous attempts to
404 link genetic lineages (Baric & Sturmbauer, 1999; Muths et al., 2009; Taboada & Pérez-Portela,
405 2016, for lineages 1 and 2) with some of the color variants identified by Koehler (1921) were
406 unsuccessful.

407 **COI divergence in ophiuroids**
408 COI K2P distances among the three clades (17.0–27.9%) were higher than the mean inter-
409 specific divergence among most ophiuroid species. In a DNA barcoding study of 503 specimens
410 of 191 ophiuroid species, Ward, Holmes & O'Hara (2008) found intra-specific variation to range
411 0–3% (mean=0.62%), whereas inter-specific divergence within genera averaged 15%. High
412 levels of genetic divergence encountered in other ophiuroid species have generally led to the
413 recognition of multiple cryptic species. Examples include the *Ophiothrix fragilis* complex: K2P
414 distance = 18.6% (Muths et al., 2009), 15–17% (Pérez-Portela, Almada & Turon, 2013), 19–22%
415 (Taboada & Pérez-Portela, 2016); *Ophioderma longicaudum* complex: K2P distance = 2.2–
416 10.2% (Boissin, Stöhr & Chenuil, 2011), 0.8–10.7% (Weber, Stöhr & Chenuil, 2019);
417 *Ophiomyxa vivipara, Ophiacantha vivipara, Ophiura ooplax, Ophiactis abyssicola* and
418 *Ophiothrix aristulata* complexes: K2P distance = 2.9–3.7%, 14.1–16.7%, 22%, 6.7%, and

419 22.9%, respectively (O'Hara et al., 2014a); and *Ophiacantha wolfarntzi* complex: K2P distance
420 = 5.4–25.7% (Martín-Ledo, Sands & López-González, 2013). The differentiation among Clades
421 1, 2, and 3 in COI is thus in line with species-level differences in other ophiuroids.

Haplotype diversity and demographic history

423 Haplotype networks display contrasting topologies, with Clades 1 and 3 showing much higher
424 intra-specific diversity than Clade 2. Clade 1 shows a great diversity of haplotypes in the
425 Northern Gulf of Mexico off Florida, where all three subclades were present. In contrast,
426 specimens from Eastern Florida, the Florida Keys, and the Southern Gulf of Mexico each fell
427 into single and different subclades. This pattern is suggestive of allopatric differentiation along
428 the periphery of the Clade's range, but few samples were available from these areas making
429 interpretation challenging. Historical demography results show evidence of recent expansion
430 (Fu's, r, SSD, and mismatches) for subclade 1A.

431 Clade 2 showed a star-like network for most specimens, evidence of recent expansion (Allcock
432 & Strugnell, 2012). Most haplotypes were within 3 m-s of the common one, except for the two
433 specimens from Guadeloupe that were 30 m-s distant. These results suggest that continental
434 populations along North and Central America are isolated from the insular population sampled in
435 the Lesser Antilles, and that the former, at least, underwent a recent expansion, potentially
436 following the Last Glacial Maximum.

437 Clade 3 showed the highest haplotype diversity and did not display signs of recent expansion in
438 all analyses but showed a high diversity of haplotypes. It is noteworthy that this is the only clade
439 that was represented among deeper water samples, suggesting that it may have the most
440 extensive depth range, and thus potentially greater physiological tolerance. The high gene
441 diversity has resulted in a larger population size than the other clades, suggesting success in
442 exploitation and colonization habitats. Some haplotypes in this clade were shared between
443 localities separated by more than 500 km.

Conclusions

445 This study provides a broad evaluation of the systematics of one of the most common ophiuroids
446 in the Tropical Western Atlantic, *Ophiothrix angulata*. COI sequence data revealed three deeply
447 divergent genetic lineages. The high color variability exhibited by this group did not correlate
448 with lineages suggesting that it represents intra-specific polymorphism. Clade 3 was separated by
449 mtDNA, nrDNA, molecular species delimitation, the shape of dorsal and ventral arm plates, and
450 the integrative analysis with mtDNA and geometric morphometric data. Therefore, we consider
451 it as a confirmed candidate species. Results demonstrate that a thorough arm morphology
452 analysis can help differentiate clades within this species complex. Molecular analyses and *in situ*
453 records show that all three clades co-occur in some areas. For Clades 1A and 2, Fu's, r, SSD, and
454 mismatches showed evidence of recent expansion. Additional geographic sampling combined
455 with physiological, reproductive, and ecological data incorporating phylogeographic analysis
456 may further resolve this species complex.

Acknowledgments

457 We thank David Pawson, Christopher Pomory, Gordon Hendler, Juan José Alvarado, and Nuno
458 Simões for their contribution with samples for sequencing. We thank Tania Pineda, Daniel
459 Janies, and Antar Pérez for their help in sequencing extra material; Tania Pineda, Carolina
460 Martín, Andrea Caballero, and Tayra Parada for images of collection labels; Berenit Mendoza
461 (Laboratorio de Microscopía Electrónica, IB-UNAM) for their technical support during the
462 acquisition of SEM images, Susana Guzmán (Laboratorio de Microscopía y Fotografía de la
463 Biodiversidad II, IB-UNAM) and Miguel Pérez (Laboratorio de Cómputo de Alto Rendimiento,
464 FC-UNAM) for their technical support; Antar Pérez (PopArt, BPP), Sandra Ospina (*geomorph*),
465 Jesús Díaz (TNT), Maite Mascaró and Dorottya Angyal for their constructive data analysis
466 advice. We thank to the museum curators and collection managers for facilitating access to their
467 collections Amanda Bemis, John Slapcinsky, Adam Baldinger, Penny Benson, Chad Walter,
468 Alicia Durán, Pedro Homa, Raúl Castillo, and Leonardo Chacón. Sequencing costs were
469 supported by NSF DEB 0529724 to GP.

References

472 Adams DC, Otárola-Castillo E. 2013. Geomorph: An R package for the collection and analysis of
473   geometric morphometric shape data. *Methods in Ecology and Evolution* 4:393–399. DOI:
474   10.1111/2041-210X.12035.

475 Allcock AL, Strugnell JM. 2012. Southern Ocean diversity: new paradigms from molecular
476   ecology. *Trends in Ecology and Evolution* 27:520–528. DOI: 10.1016/j.tree.2012.05.009.

477 Alvarado JJ, Solís-Marín FA (eds.). 2013. *Echinoderms research and diversity in Latin America*.
478   Berlin: Springer.

479 Alvarado JJ, Solís-Marín FA, Ahearn C. 2008. Equinodermos (Echinodermata) del Caribe
480   Centroamericano. *Revista de Biología Tropical* 56:37–55.

481 Arlyza IS, Shen KN, Solihin DD, Soedharma D, Berrebi P, Borsa P. 2013. Species boundaries in
482   the *Himantura uarnak* species complex (Myliobatiformes: Dasyatidae). *Molecular*
483   *Phylogenetics and Evolution* 66:429–435. DOI: 10.1016/j.ympev.2012.09.023.

484 Aronson RB. 1988. Palatability of five Caribbean ophiuroids. *Bulletin of Marine Science* 43:93–
485   97.

486 Bailey RC, Byrnes J. 1990. A new, old method for assessing measurement error in both univariate
487   and multivariate morphometric studies. *Systematic Zoology* 39:124–130.

488 Baric S, Sturmbauer C. 1999. Ecological parallelism and cryptic species in the genus *Ophiothrix*
489   derived from mitochondrial DNA sequences. *Molecular Phylogenetics and Evolution* 11:157–
490   162.

491 Benavides-Serrato M, O'Hara TD. 2008. A new species in the *Ophiocoma erinaceus* complex
492   from the South-west Pacific Ocean (Echinodermata: Ophiuroidea: Ophiocomidae). *Memoirs of*
493   *Museum Victoria* 65:51–56. DOI: 10.24199/j.mmv.2008.65.4.

494 Benítez HA, Avaria-Llautureo J, Canales-Aguirre CB, Jerez V, Parra LE, Hernández CE. 2013.
495   Evolution of sexual size dimorphism and its relationship with sex ratio in carabid beetles of
496   Genus *Ceroglossus* Solier. *Current Zoology* 59:769–777. DOI: 10.1093/czoolo/59.6.769.

497 Bickford D, Lohman DJ, Sodhi NS, Ng PKL, Meier R, Winker K, Ingram KK, Das I. 2007.
498   Cryptic species as a window on diversity and conservation. *Trends in ecology & evolution*
499   22:148-155. DOI: 10.1016/j.tree.2006.11.004.

500 Boissin E, Féral JP, Chenuil A. 2008. Defining reproductively isolated units in a cryptic and
501   syntopic species complex using mitochondrial and nuclear markers: the brooding brittle star,
502   *Amphipholis squamata* (Ophiuroidea). *Molecular Ecology* 17:1732-1744. DOI: 10.1111/j.1365-
503   294X.2007.03652.x.

504 Boissin E, Hoareau TB, Paulay G, Bruggemann JH. 2016. Shallow-water reef ophiuroids
505   (Echinodermata: Ophiuroidea) of Réunion (Mascarene Islands), with biogeographic
506   considerations. *Zootaxa* 4098:273. DOI: 10.11646/zootaxa.4098.2.4.

507 Boissin E, Stöhr S, Chenuil A. 2011. Did vicariance and adaptation drive cryptic speciation and
508   evolution of brooding in *Ophioderma longicauda* (Echinodermata: Ophiuroidea), a common
509   Atlanto-Mediterranean ophiuroid?. *Molecular Ecology* 20:4737–4755. DOI: 10.1111/j.1365-
510   294X.2011.05309.x.

511 Borrero-Pérez GH, Benavides-Serrato M, Solano Ó, Navas S GR. 2008. Brittle-stars
512   (Echinodermata: Ophiuroidea) from the continental shelf and upper slope of the Colombian
513   Caribbean. *Revista de Biologia Tropical* 56:169–204.

514 Clark HL. 1901. The Echinoderms of Porto Rico. *U.S. Fish Commission Bulletin for 1900* 2:231–
515   263.

516 Clark HL. 1918. Brittle-stars, new and old. *Bulletin of the Museum of Comparative of Zoology at*
517   *Harvard College* 62:265–338.

518 Clark HL. 1933. *Scientific Survey of Porto Rico and the Virgin Islands*. New York: New York
519   Academy of Sciences.

520 Clark HL. 1946. Family Ophiotrichidae. In: *The echinoderm fauna of Australia. Its Composition*
521   *and its origin*. Washington, D.C.: Carnegie Institution of Washington Publication, 213–228.

522 Clark AM. 1967. Notes on the family ophiotrichidae (Ophiuroidea). *Journal of Natural History*
523   *Series 13* 9:637–655. DOI: 10.1080/00222936608651676.

524 Clement M, Snell Q, Walker P, Posada D, Crandall K. 2002. TCS: Estimating gene genealogies.
525   In: *Parallel and Distributed Processing Symposium, International Proceedings* 184.

526 Darriba D, Taboada GL, Doallo R, Posada D. 2012. JModelTest 2: More models, new heuristics
527   and parallel computing. *Nature Methods* 9:772. DOI: 10.1038/nmeth.2109.

528 De los Palos-Peña M, Solís-Marín FA, Laguarda-Figueras A, Durán-González A. 2021.
529   Ontogenetic variation of the odontophore of *Luidia superba* (Asteroidea: Paxillosida) and its

530   taxonomic implications. *Revista de Biología Tropical* 69:89-100. DOI:
531   10.15517/rbt.v69iSuppl.1.46330.

532 Devaney DM. 1974. Shallow-water echinoderms from British Honduras, with a description of a
533   new species of *Ophiocoma* (Ophiuroidea). *Bulletin of Marine Science* 22:122–164.

534 Dryden IL. 2018. Shapes package. R Foundation for Statistical Computing, Vienna, Austria.
535   Contributed package, version 1.2.4.

536 Edgar RC. 2004. MUSCLE: Multiple sequence alignment with high accuracy and high
537   throughput. *Nucleic Acids Research* 32:1792–1797. DOI: 10.1093/nar/gkh340.

538 Excoffier L, Lischer HEL. 2010. Arlequin suite version 3.5: A new series of programs to perform
539   population genetics analyses under Linux and Windows. *Molecular Ecology Resources*
540   10:564–567. DOI: 10.1111/j.1755-0998.2010.02847.x.

541 Felsenstein J. 1985. Confidence limits on phylogenies: An approach using the bootstrap. *Evolution*
542   39:783–791.

543 Fox J, Weisberg S, Price B. 2018. Car: Companion to Applied Regression. R Package version 3.0-
544   2. Available online at: https://CRAN.R-project.org/package=car (2020).

545 Fu YX. 1997. Statistical tests of neutrality of mutations against population growth, hitchhiking
546   and background selection. *Genetics Society of America* 147:915–925.

547 GBIF: *Ophiothrix angulata* (Say, 1825) in GBIF Secretariat (2022). GBIF Backbone Taxonomy.
548   Checklist dataset https//doi.org/10.15468/39omei accessed via GBIF.org on May 26th, 2022.

549 Goloboff PA, Catalano SA. 2016. TNT version 1.5, including a full implementation of
550   phylogenetic morphometrics. *Cladistics* 32:221–238.

551 Harpending HC. 1994. Signature of Ancient Population Growth in a Low-Resolution
552   Mitochondrial DNA Mismatch Distribution. *Human Biology* 66:591–600.

553 Hendler G. 2005. Two new brittle star species of the genus *Ophiothrix* (Echinodermata:
554   Ophiuroidea: Ophiotrichidae) from coral reefs in the Southern Caribbean Sea, with notes on
555   their biology. *Caribbean Journal of Science* 41:583–599.

556 Hendler G, Baldwin CC, Smith DG, Thacker CE. 1999. Planktonic dispersal of juvenile brittle
557   stars (Echinodermata: Ophiuroidea) on a Caribbean reef. *Bulletin of Marine Science* 65:283–
558   288.

559 Hendler G, Littman BS. 1986. The ploys of sex: relationships among the mode of reproduction,
560   body size and habitats of coral-reef brittlestars. *Coral Reefs* 5:31–42. DOI:
561   10.1007/BF00302169.

562 Hendler G, Miller JE, Pawson DL, Kier PM. 1995. *Echinoderms of Florida and the Caribbean:*
563   *Sea stars, sea urchins, and allies*. Washington, D.C.: Smithsonian Institution Press.

564 Herrera-Moreno A, Betancourt Fernández L. 2004. Especies de equinodermos recientes
565   (Echinodermata: Crinoidea, Asteroidea, Ophiuroidea, Echinoidea y Holothuroidea) conocidas
566   para la Hispaniola. *Revista Ciencia y Sociedad* 29:506–533.

567 Hoareau TB, Boissin E. 2010. Design of phylum-specific hybrid primers for DNA barcoding:
568   addressing the need for efficient COI amplification in the Echinodermata. *Molecular Ecology*
569   *Resources* 10:960–967. DOI: 10.1111/j.1755-0998.2010.02848.x.

570 Hoareau TB, Boissin E, Paulay G, Bruggemann JH. 2013. The Southwestern Indian Ocean as a
571   potential marine evolutionary hotspot: perspectives from comparative phylogeography of reef
572   brittle-stars. *Journal of Biogeography* 40:2167–2179. DOI: 10.1111/jbi.12155.

573 Hoggett AK. 1991. The genus *Macrophiothrix* (Ophiuroidea: Ophiotrichidae) in Australian
574   waters. *Invertebrate Taxonomy* 4:1077–1146. DOI: 10.1071/IT9901077.

575 Kapli P, Lutteropp S, Zhang J, Kobert K, Pavlidis P, Stamatakis A, Flouri T. 2017. Multi-rate
576   Poisson tree processes for single-locus species delimitation under maximum likelihood and
577   Markov chain Monte Carlo. *Bioinformatics* 33:1630–1638. DOI:
578   10.1093/bioinformatics/btx025.

579 Kearse M, Moir R, Wilson A, Stones-Havas S, Cheung M, Sturrock S, Buxton S, Cooper A,
580   Markowitz S, Duran C, Thierer T, Ashton B, Meintjes P, Drummond A. 2012. Geneious Basic:
581   An integrated and extendable desktop software platform for the organization and analysis of
582   sequence data. *Bioinformatics* 28:1647–1649. DOI: 10.1093/bioinformatics/bts199.

583 Kimura M. 1980. A simple method for estimating evolutionary rates of base substitutions through
584   comparative studies of nucleotide sequences. *Journal of Molecular Evolution* 16:111–120.
585   DOI: 10.1007/BF01731581.

586 Kissling DL, Taylor GT. 1977. Habitat factors for reef dwelling ophiuroids in the Florida Keys.
587   In: Symposium RS of M and A ed. *Third International Coral Reef Symposium*. Miami, Florida:
588   University of Miami, 225–231.

589 Klingenberg CP. 2016. Size, shape, and form: concepts of allometry in geometric morphometrics.
590   *Development Genes and Evolution* 226:113–137. DOI: 10.1007/s00427-016-0539-2.

591 Klingenberg CP. 2022. Methods for studying allometry in geometric morphometrics: a
592   comparison of performance. *Evolutionary Ecology* 36:439-470. DOI: 10.1007/s10682-022-
593   10170-z

594 Koehler R. 1921. *Faune de France. 1. Echinodermes*. Paris.

595 Laguarda-Figueras A, Hernández-Herrejón LA, Solís-Marín FA, Durán-González A. 2009.
596   *Ofiuroideos del Caribe mexicano y Golfo de México*. ICML-UNAM, CONABIO, México.

597 Leigh JW, Bryant D. 2015. POPART: Full-feature software for haplotype network construction.
598   *Methods in Ecology and Evolution* 6:1110–1116. DOI: 10.1111/2041-210X.12410.

599 Lewis J, Bray R. 1983. Community structure of ophiuroids (Echinodermata) from three different
600   habitats on a coral reef in Barbados, West Indies. *Marine Biology* 73:171–176.

601 Ljungman A. 1867. Ophiuroidea viventia huc usque cognita enumerat. *Öfversigt af Kgl.*
602   *Vetenskaps-Akademiens Förhandlingar* 23:303–336.

603 Luo A, Ling C, Ho SYW, Zhu CD. 2018. Comparison of methods for molecular species
604   delimitation across a range of speciation scenarios. *Systematic Biology* 67:830–846. DOI:
605   10.1093/sysbio/syy011.

606 Lütken CF. 1856. Bidrag til Kundskab om Slangestjernerne. II. Oversigt over de vestindiske
607   Ophiurer. *Videnskabelige Meddelelser fra Dansk Naturhistorisk Förening i Kjøbenhavn* 7:1–
608   19.

609 Lyman T. 1860. Descriptions of new Ophiuridae, belonging to the Smithsonian Institution and to
610   the Museum of Comparative Zoology at Cambridge. *Proceedings of the Boston Society of*
611   *Natural History* 1859–61:193–204.

612 Lyman T. 1865. *Ophiothrix angulata*. In: *Ophiuridae and Astrophytidae*. University Press,
613   Cambridge, Welch, Bigelow & Co., 162–164.

614 Maddison WP, Maddison DR. 2018. Mesquite: a modular system for evolutionary analysis.
615   Version 3.51.

616 Martín-Ledo R, Sands CJ, López-González PJ. 2013. A new brooding species of brittle star
617   (Echinodermata: Ophiuroidea) from Antarctic waters. *Polar Biology* 36:115–126. DOI:
618   10.1007/s00300-012-1242-z.

619 Martínez-Melo A, De Luna E, Buitrón-Sánchez BE. 2017. Morfometría de los equinodeos de la
620   Familia Cassidulidae (Echinoidea: Cassiduloida). *Revista de Biología Tropical* 65:S233-S243.
621   DOI: 10.15517/rbt.v65i1-1.31691.

622 Masonick P, Weirauch C. 2019. Integrative species delimitation in Nearctic ambush bugs
623   (Heteroptera: Reduviidae: Phymatinae): insights from molecules, geometric morphometrics and
624   ecological associations. *Systematic Entomology* 45:205–223. DOI: 10.1111/syen.12388.

625 Michonneau F, Paulay G. 2014. Revision of the genus *Phyrella* (Holothuroidea: Dendrochirotida)
626   with the description of a new species from Guam. *Zootaxa* 3760:101–140. DOI:
627   10.11646/zootaxa.3760.2.1.

628 Miller MA, Pfeiffer W, Schwartz T. 2010. Creating the CIPRES Science gateway for inference of
629   large phylogenetic trees. In: *Proceedings of the Gateway Computing Environments Workshop*
630   *(GCE)*. New Orleans, L.A. 1–8. DOI: 10.1109/GCE.2010.5676129

631 Moritz CC, Pratt RC, Bank S, Bourke G, Bragg JG, Doughty P, Keogh JS, Laver RJ, Potter S,
632   Teasdale LC, Tedeschi LG, Oliver PM. 2018. Cryptic lineage diversity, body size divergence,
633   and sympatry in a species complex of Australian lizards (*Gehyra*). *Evolution* 72:54–66. DOI:
634   10.1111/evo.13380.

635 Müller K, Müller J, Neinhuis C, Quandt D. 2010. PhyDE–Phylogenetic Data Editor, version
636   0.9971. Program distributed by the authors. http:\\www.phyde.de.

637 Müller J, Troschel FH. 1842. System der Asteriden.1. Asteriae. 2. Ophiuridae. *Vieweg:*
638   *Braunschweig*:115.

639 Muths D, Jollivet D, Gentil F, Davoult D. 2009. Large-scale genetic patchiness among NE
640   Atlantic populations of the brittle star *Ophiothrix fragilis*. *Aquatic Biology* 5:117–132. DOI:
641   10.3354/ab00138.

642 Naughton KM, O'Hara TD, Appleton B, Cisternas PA. 2014. Antitropical distributions and
643   species delimitation in a group of ophiocomid brittle stars (Echinodermata: Ophiuroidea:
644   Ophiocomidae). *Molecular Phylogenetics and Evolution* 78:232–244. DOI:
645   10.1016/j.ympev.2014.05.020.

646 Newton LG, Starrett J, Hendrixson BE, Derkarabetian S, Bond JE. 2020. Integrative species
647   delimitation reveals cryptic diversity in the southern Appalachian *Antrodiaetus unicolor*
648   (Araneae: Antrodiaetidae) species complex. *Molecular Ecology* 2:2269-2287. DOI:
649   10.1111/mec.15483

650 Noriega N, Fuentes-Carrero Y. 2014. Contribución al conocimiento de la diversidad de los
651   equinodermos del Parque Nacional Archipiélago de Los Roques, Venezuela. *Acta Biologica*
652   *Venezuelica* 34:285–292.

653 O'Hara TD, England PR, Gunasekera RM, Naughton KM. 2014a. Limited phylogeographic
654   structure for five bathyal ophiuroids at continental scales. *Deep Sea Research Part I:*
655   *Oceanographic Research Papers* 84:18–28. DOI: 10.1016/j.dsr.2013.09.009.

656 O'Hara TD, Hugall AF, Thuy B, Moussalli A. 2014b. Phylogenomic resolution of the Class
657   Ophiuroidea unlocks a global microfossil record. *Current Biology* 24:1874-1879. DOI:
658   10.1016/j.cub.2014.06.060.

659 O'Hara TD, Hugall AF, Thuy B, Stöhr S, Martynov AV. 2017. Restructuring higher taxonomy
660   using broad-scale phylogenomics: The living Ophiuroidea. *Molecular Phylogenetics and*
661   *Evolution* 107:415–430. DOI: 10.1016/j.ympev.2016.12.006.

662 O'Hara TD, Stöhr S, Hugall AF, Thuy B, Martynov A. 2018. Morphological diagnoses of higher
663   taxa in Ophiuroidea (Echinodermata) in support of a new classification. *European Journal of*
664   *Taxonomy* 416:1–35. DOI: 10.5852/ejt.2018.416.

665 Padial JM, Miralles A, de la Riva I, Vences M. 2010. The integrative future of taxonomy.
666   *Frontiers in Zoology* 7:1–14. DOI: 10.1186/1742-9994-7-16.

667 Pérez-Portela R, Almada V, Turon X. 2013. Cryptic speciation and genetic structure of widely
668   distributed brittle stars (Ophiuroidea) in Europe. *Zoologica Scripta* 42:151–169. DOI:
669   10.1111/j.1463-6409.2012.00573.x.

670 Rambaut A. 2018. FigTree version 1.4.4. Institute of Evolutionary Biology, University of
671   Edinburgh, Edinburgh, U.K.

672 Rambaut A, Drummond AJ, Xie D, Baele G, Suchard MA. 2018. Posterior summarization in
673   Bayesian Phylogenetics using Tracer 1.7. *Systematic Biology* 67:901–904. DOI:
674   10.1093/sysbio/syy032.

675 Richards VP, DeBiasse MB, Shivji MS. 2015. Genetic evidence supports larval retention in the
676   Western Caribbean for an invertebrate with high dispersal capability (*Ophiothrix suensonii*:
677   Echinodermata, Ophiuroidea). *Coral Reefs* 34:313–325. DOI: 10.1007/s00338-014-1237-z.

678 Rohlf FJ. 2013. *tpsDIG, digitize landmarks and outlines, version 2.17*. Department of Ecology and
679   Evolution, State University of New York at Stony Brook.

680 Ronquist F, Teslenko M, Van Der Mark P, Ayres DL, Darling A, Höhna S, Larget B, Liu L,
681   Suchard MA, Huelsenbeck JP. 2012. MrBayes version 3.2: efficient Bayesian phylogenetic
682   inference and model choice across a large model space. *Systematic biology* 61:539–542. DOI:
683   10.1093/sysbio/sys029.

684 Rozas J, Ferrer-Mata A, Sánchez-DelBarrio JC, Guirao-Rico S, Librado P, Ramos-Onsins SE,
685   Sánchez-Gracia A. 2017. DnaSP 6: DNA Sequence Polymorphism Analysis of Large Datasets.
686   *Molecular Biology and Evolution* 34:3299–3302.

687 Sandino OB, Solís-Marín FA, Caballero-Ochoa AA, Conejeros-Vargas CA, Márquez-Borrás F,
688   Ayala-Aguilera AP, Laguarda-Figueras A. 2017. Equinodermos de Nicaragua: nuevos registros
689   del Pacífico y Caribe Sur. *Revista de Biología Tropical* 65:S288–S298.

690 Santana A, Manso CLC, Almeida ACS, Alves OFS. 2017. Redescription and designation of a
691   neotype for *Ophiothrix angulata* (Say, 1825) (Echinodermata: Ophiuroidea: Ophiotrichidae).
692   *Zootaxa* 4344:291–307. DOI: 10.11646/zootaxa.4344.2.5.

693 Santana A, Manso CLC, Almeida ACS, Alves OFS. 2020. Taxonomic review of *Ophiothrix*
694   Müller & Troschel, 1840 (Echinodermata: Ophiuroidea) from Brazil, with the description of
695   four new species. *Zootaxa* 4808:51–78. DOI: 10.11646/zootaxa.4808.1.3.

696 dos Santos Alitto RA, Zacagnini Amaral AC, Dias de Oliveira L, Serrano H, Seger KR, Borges
697   Guilherme PD, Di Domenico M, Christensen AB, Bolsoni Lourenço L, Tavares M, Borges M.
698   2019. Atlantic west *Ophiothrix* spp. In the scope of integrative taxonomy: Confirming the
699   existence of *Ophiothrix trindadensis* Tommasi, 1970. *PLoS ONE* 14:1–28. DOI:
700   10.1371/journal.pone.0210331.

701 Say T. 1825. On the species of the Linnean genus *Aterias*, inhabiting the coast of the United
702   States. *Journal of the Academy of Natural Sciences of Philadelphia* 5:141–154.

703 Sobha TR, Vibija CP, Fahima P. 2023. Coral Reef: A Hot Spot of Marine Biodiversity. In:
704   Sukumaran, S.T., T R, K. (eds) *Conservation and Sustainable Utilization of Bioresources.*
705   *Sustainable Development and Biodiversity*. Springer, Singapore. https://doi.org/10.1007/978-
706   981-19-5841-0_8

707 Solís-Lemus C, Knowles LL, Ané C. 2015. Bayesian species delimitation combining multiple
708   genes and traits in a unified framework. *Evolution* 69:492–507. DOI: 10.1111/evo.12582.

709 Stamatakis A. 2006. RAxML-VI-HPC: Maximum likelihood-based phylogenetic analyses with
710   thousands of taxa and mixed models. *Bioinformatics* 22:2688–2690. DOI:
711   10.1093/bioinformatics/btl446.

712 Stamatakis A, Hoover P, Rougemont J. 2008. A rapid bootstrap algorithm for the RAxML web
713   servers. *Systematic Biology* 57:758–771. DOI: 10.1080/10635150802429642.

714 Stöhr S. 2005. Who's who among baby brittle stars (Echinodermata: Ophiuroidea):
715   Postmetamorphic development of some North Atlantic forms. *Zoological Journal of the*
716   *Linnean Society* 143:543–576. DOI: 10.1111/j.1096-3642.2005.00155.x.

717 Stöhr S, O'Hara TD, Thuy B. 2012. Global Diversity of Brittle Stars (Echinodermata:
718   Ophiuroidea). *PLoS ONE* 7:e31940. DOI: 10.1371/journal.pone.0031940.

719 Stöhr S, O'Hara TD, Thuy B. 2023. World Ophiuroidea Database. *Available at*
720   *http://www.marinespecies.org/ophiuroidea* (accessed April 16th, 2023). DOI: 10.14284/358.

721 Swisher RE. 2021. Convergent discoidal sand dollars from isolated regions: A geometric
722   morphometric analyses of *Dendraster* and *Arachnoides*. *Terrestrial Atmospheric and Oceanic*
723   *Sciences* 32:1117-1130.

724 Taboada S, Pérez-Portela R. 2016. Contrasted phylogeographic patterns on mitochondrial DNA of
725   shallow and deep brittle stars across the Atlantic-Mediterranean area. *Scientific Reports*
726   6:32425. DOI: 10.1038/srep32425.

727 Tajima F. 1989. Statistical method for testing the neutral mutation hypothesis by DNA
728   polymorphism. *Genetics Society of America* 123:585–595.

729 Tamura K, Stecher G, Kumar S. 2021. MEGA11: Molecular Evolutionary Genetics Analysis
730   Version 11. *Molecular Biology and Evolution* 38:3022–3027. DOI: 10.1093/molbev/msab120.

731 Thuy B, Stöhr S. 2011. Lateral arm plate morphology in brittle stars (Echinodermata:
732   Ophiuroidea): new perspectives for ophiuroid micropalaeontology and classification. *Zootaxa*
733   3013:1-47. DOI: 10.11646/zootaxa.3013.1.1.

734 Thuy B, Stöhr S. 2016. A new morphological phylogeny of the Ophiuroidea (Echinodermata)
735   accords with molecular evidence and renders microfossils accessible for cladistics. *PLoS ONE*
736   11: e0156140. DOI: 10.1371/journal.pone.0156140.

737 Tommasi LR. 1970. *Os ofiuróides recentes do Brasil e de regiões vizinhas*. Universidade de São
738   Paulo. Instituto oceanográfico.

739 del Valle García R, Abreu Pérez M, Rodríguez R, Solís-Marín FA, Laguarda-Figueras A, Durán-
740   González A. 2008. Equinodermos (Echinodermata) del occidente del Archipiélago Sabana-
741   Camagüey, Cuba. *Revista de Biología Tropical* 56:19–35.

742 Vermeij GJ. 2005. One-way traffic in the western Atlantic: causes and consequences of Miocene
743   to early Pleistocene molluscan invasions in Florida and the Caribbean. *Paleobiology* 31:624–
744   642. DOI: 10.1666/0094-8373(2005)031[0624:OTITWA]2.0.CO;2.

745 Verrill AE. 1899. Report on the Ophiuroidea collected by the Bahama Expedition in 1893.
746   *Bulletin from the Laboratories of Natural History of the State University of Iowa.* 5:1-86. pls. I-
747   VIII.

748 Viscosi V, Cardini A. 2011. Leaf morphology, taxonomy and geometric morphometrics: A
749   simplified protocol for beginners. *PLoS ONE* 6. DOI: 10.1371/journal.pone.0025630.

750 Walsh PS, Metzger DA, Higuchi R. 1991. Chelex 100 as a medium for simple extraction of DNA
751   for PCR-based typing from forensic material. *Biotechniques* 10:506–513.

752 Ward RD, Holmes BH, O'Hara TD. 2008. DNA barcoding discriminates echinoderm species.
753   *Molecular Ecology Resources* 8:1202–1211. DOI: 10.1111/j.1755-0998.2008.02332.x.

754 Weber AAT, Stöhr S, Chenuil A. 2019. Species delimitation in the presence of strong incomplete
755   lineage sorting and hybridization: Lessons from *Ophioderma* (Ophiuroidea: Echinodermata).
756   *Molecular Phylogenetics and Evolution* 131:138–148. DOI: 10.1016/j.ympev.2018.11.014.

757 Wickham H. 2016. *ggplot2: Elegant Graphics for Data Analysis*. Springer-Verlag, New York.

758 Yang Z. 2015. The BPP program for species tree estimation and species delimitation. *Current*
759   *Zoology* 61:854–865. DOI: 10.1093/czoolo/61.5.854.

760 Yang Z, Rannala B. 2010. Bayesian species delimitation using multilocus sequence data.
761   *Proceedings of the National Academy of Sciences of the United States of America* 107:9264–
762   9269. DOI: 10.1073/pnas.0913022107.

763 Yezerinac SM, Lougheed SC, Handford P. 1992. Measurement error and morphometric studies:
764   Statistical power and observer experience. *Systematic Biology* 41: 471–482. DOI:
765   10.1093/sysbio/41.4.471.

766 Zhang J, Kapli P, Pavlidis P, Stamatakis A. 2013. A general species delimitation method with
767   applications to phylogenetic placements. *Bioinformatics* 29: 2869–2876. DOI:
768   10.1093/bioinformatics/btt499.

Figure 1

Sampling locations with the proportion of specimens per clade are given as pie charts.

Sampling locations (see Table S1 for details), with the proportion of specimens per clade given as pie charts. Clade 1 (green), Clade 2 (blue), and Clade 3 (pink). OS: off Steinhatchee, North of St. Petersburg and Cedar Key. NWSP: Northwest of St. Petersburg. NSP and SSP: North and South of St. Petersburg. NFK: North of Florida Keys. FK: Florida Keys. PB: Palm Beach. JA: near Jacksonville. LU: near Louisiana. TV: Tuxpan Veracruz. SV: Sistema Arrecifal Veracruzano and Monte Pio. CAC: Cayo Arcas area. CAN: Cayo Arenas. ALA: Alacranes Reef. MR: Mayan Riviera. MH: Mahahual. BE: Belize. NI: Nicaragua. CR: Costa Rica. PA: Panama. StM: St. Martin. CU: Curaçao. GU: Guadeloupe. FG: French Guiana. © OpenStreetMap 2022.
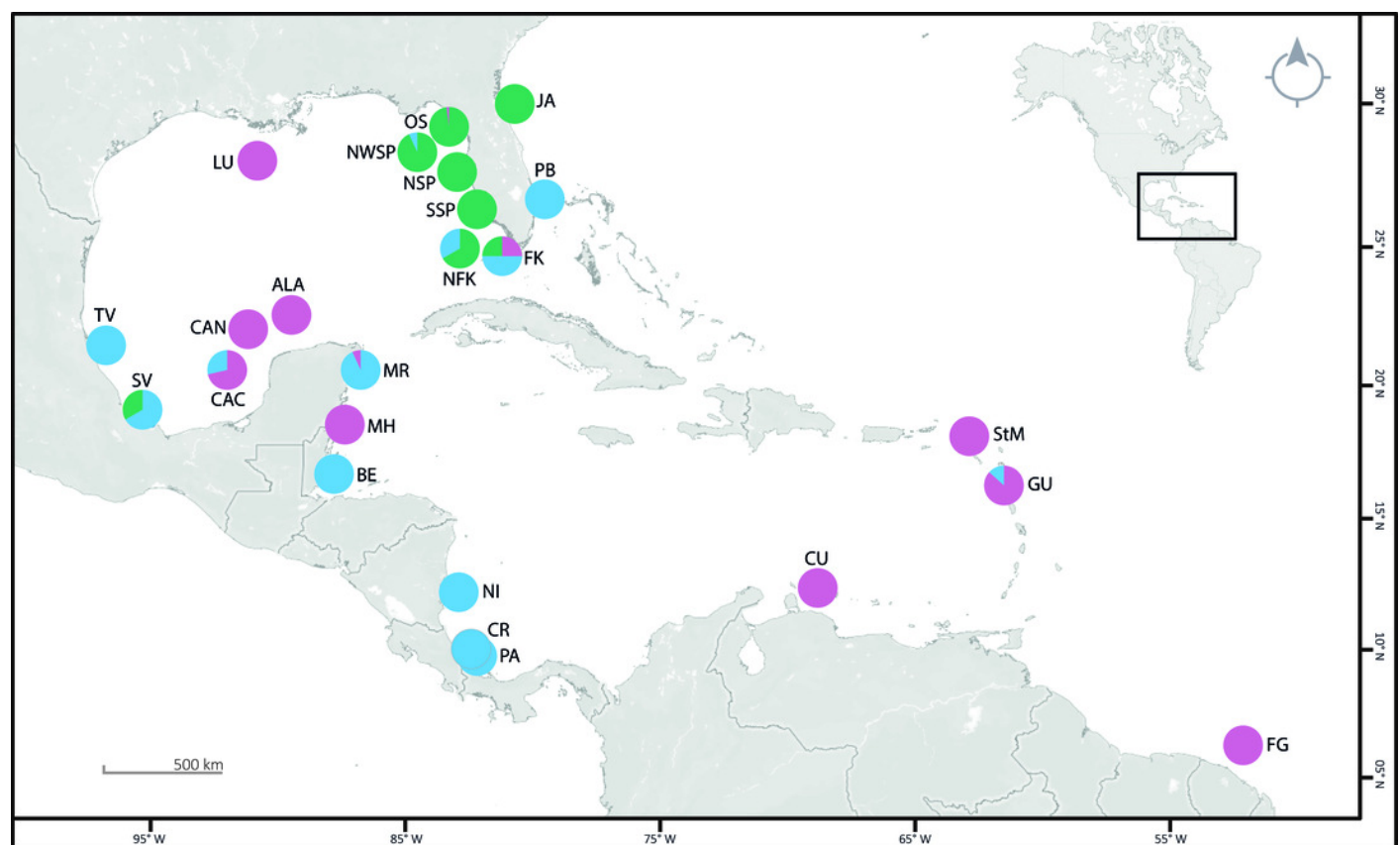
Figure 2

DAP and VAP landmarks

Landmarks type II (red) and semi-landmarks (yellow) used for geometric morphometrics to investigate variation in arm plates in *Ophiothrix angulata*. Numbers indicate landmark position. (A) Dorsal arm plate (DAP). (B) Ventral arm plate (VAP). Pe: Proximal edge. De: Distal edge. Photos credit: Y. Quetzalli Hernández-Díaz.
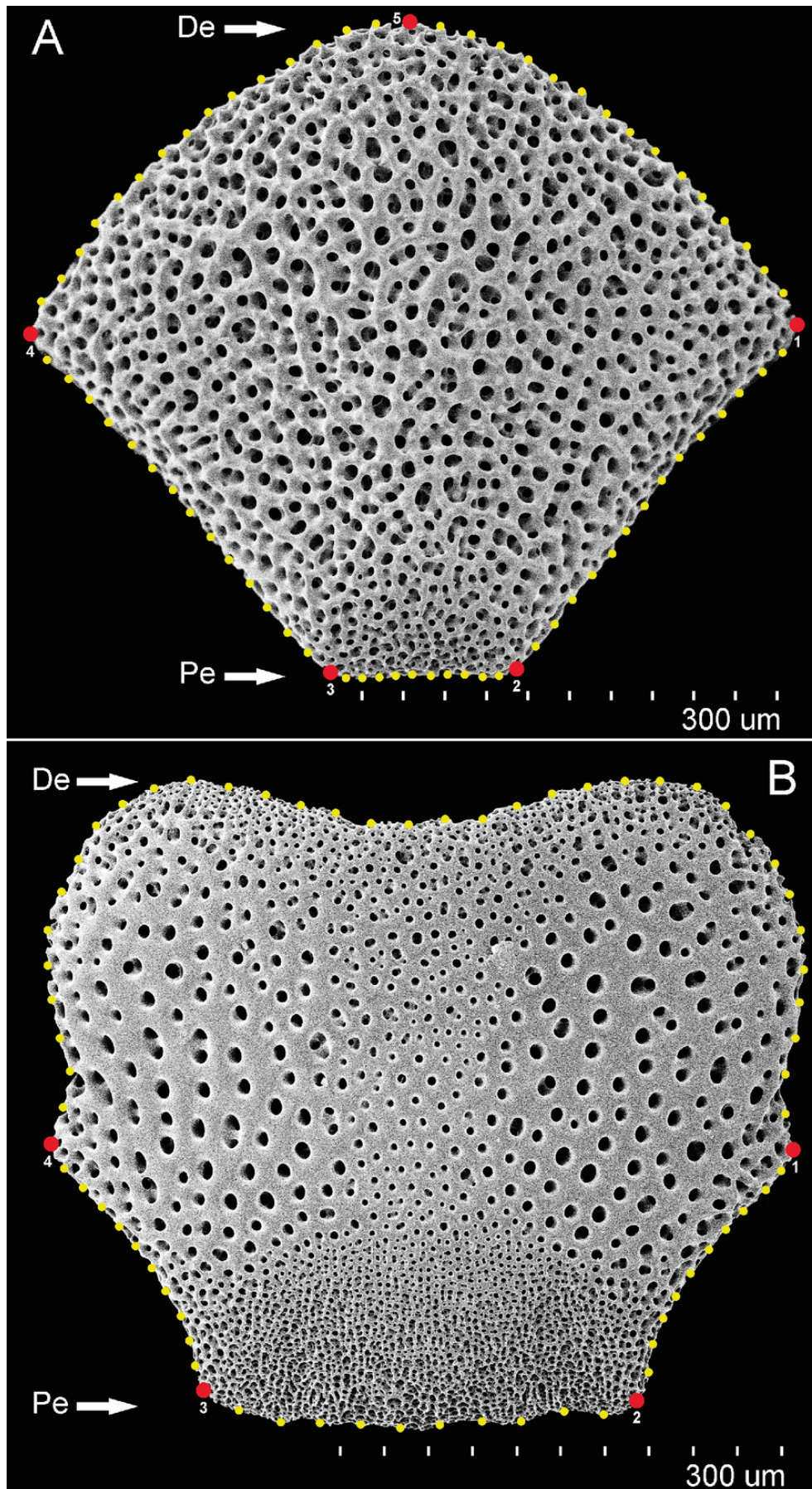
Figure 3

mtDNA bayesian consensus tree

Bayesian consensus tree of COI sequences produced using the GTR+I+G model in MrBayes v.3.2.7a on XSEDE for *Ophiothrix angulata* and outgroups. Clade 1 (green), Clade 2 (blue), Clade 3 (pink), and Outgroup (gray). Bayesian posterior probabilities (above), followed by ML bootstrap support (below; 1,000 replicates), are indicated at nodes.
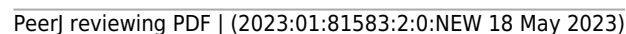
Figure 4

mtDNA vs nrDNA trees

A comparison of mtDNA (COI) (left) and nrDNA (ITS-2) (right) phylogenies from the BI analysis are displayed as cladograms for *Ophiothrix angulata* with Bayesian posterior probabilities displayed above and ML bootstrap (1,000 replicates) support displayed below the nodes.
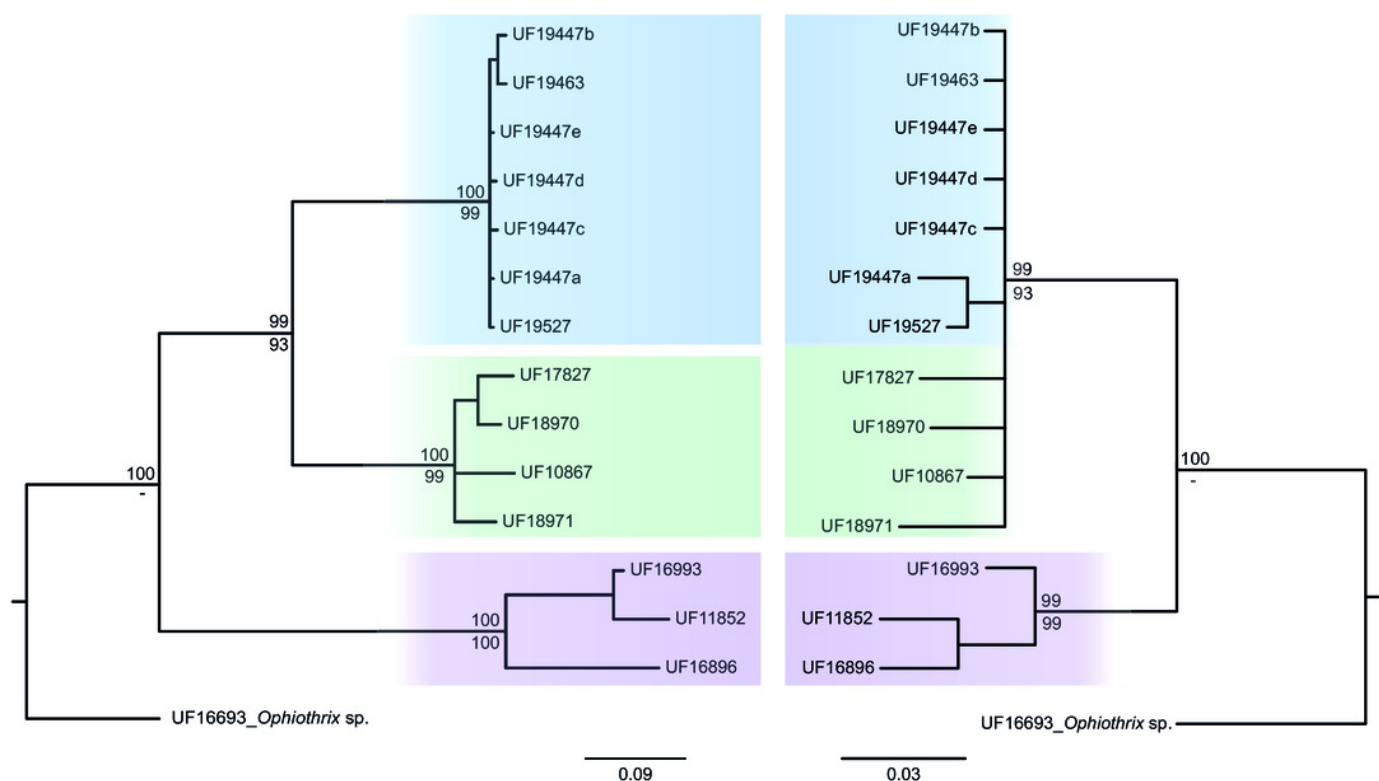
Figure 5

TCS haplotype network clades 1 and 2

Clades 1 and 2. Clade 1A (n=42), Clade 1B (n=26), Clade 1C (n=3), Clade 2A (n=42), and Clade 2B (n=2). TCS haplotype network of COI sequences for two *Ophiothrix angulata* clades (632 bp). The number of specimens is superimposed onto the more abundant haplotypes. Northern Gulf of Mexico (green). Florida Keys (orange). Eastern Florida (vermilion). Southern Gulf of Mexico (grey). Campeche Bank (yellow). Western Caribbean (blue). Southwestern Caribbean (sky blue). Eastern Caribbean (pink).
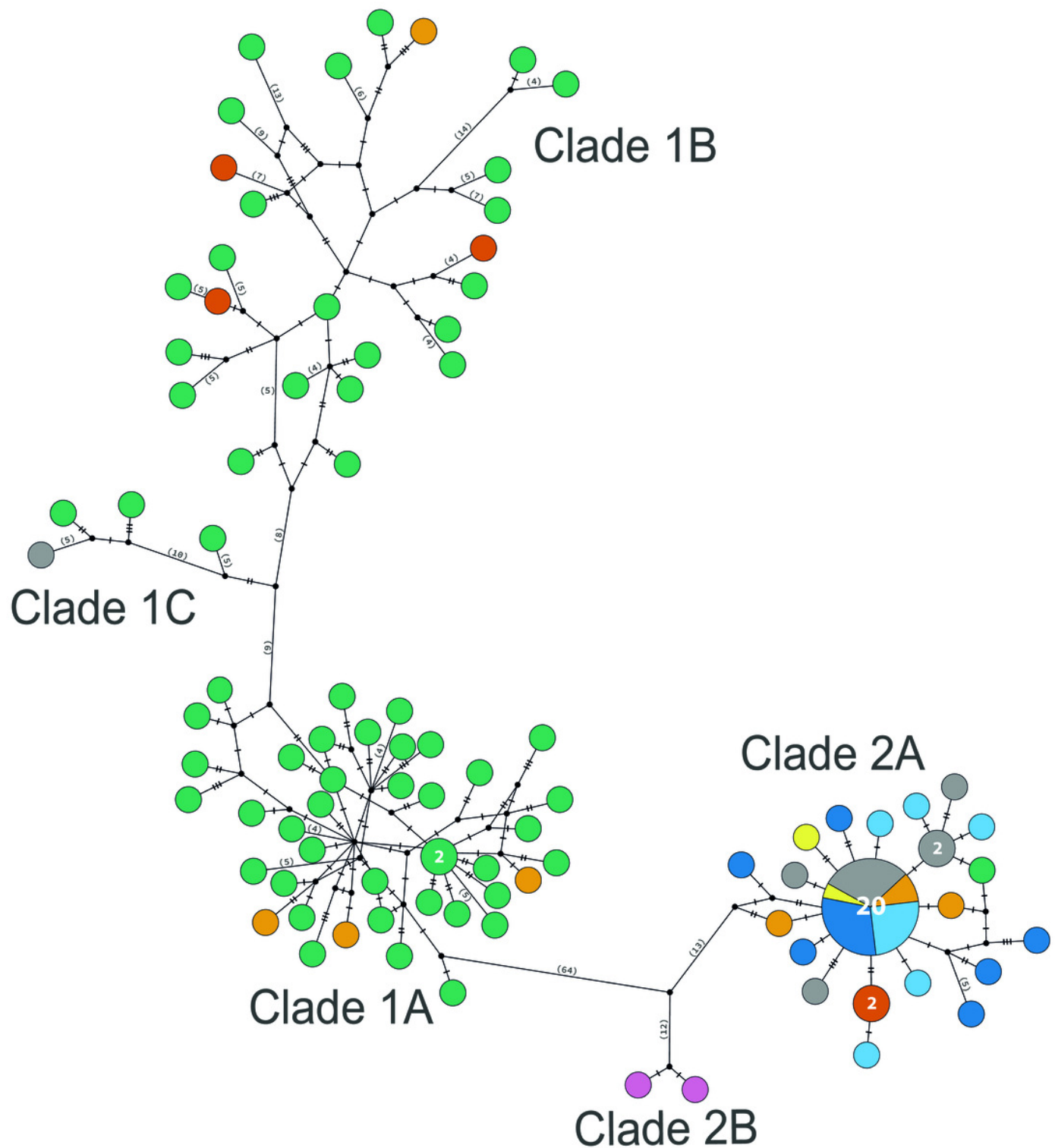
Figure 6

TCS haplotype network Clade 3

Clade 3 (n=31). TCS haplotype network of COI sequences for one *Ophiothrix angulata* clade (632 pb). The number of specimens is superimposed onto the more abundant haplotypes. Northern Gulf of Mexico (green). Florida Keys (orange). Campeche Bank (yellow). Western Caribbean (blue). Eastern Caribbean (pink).
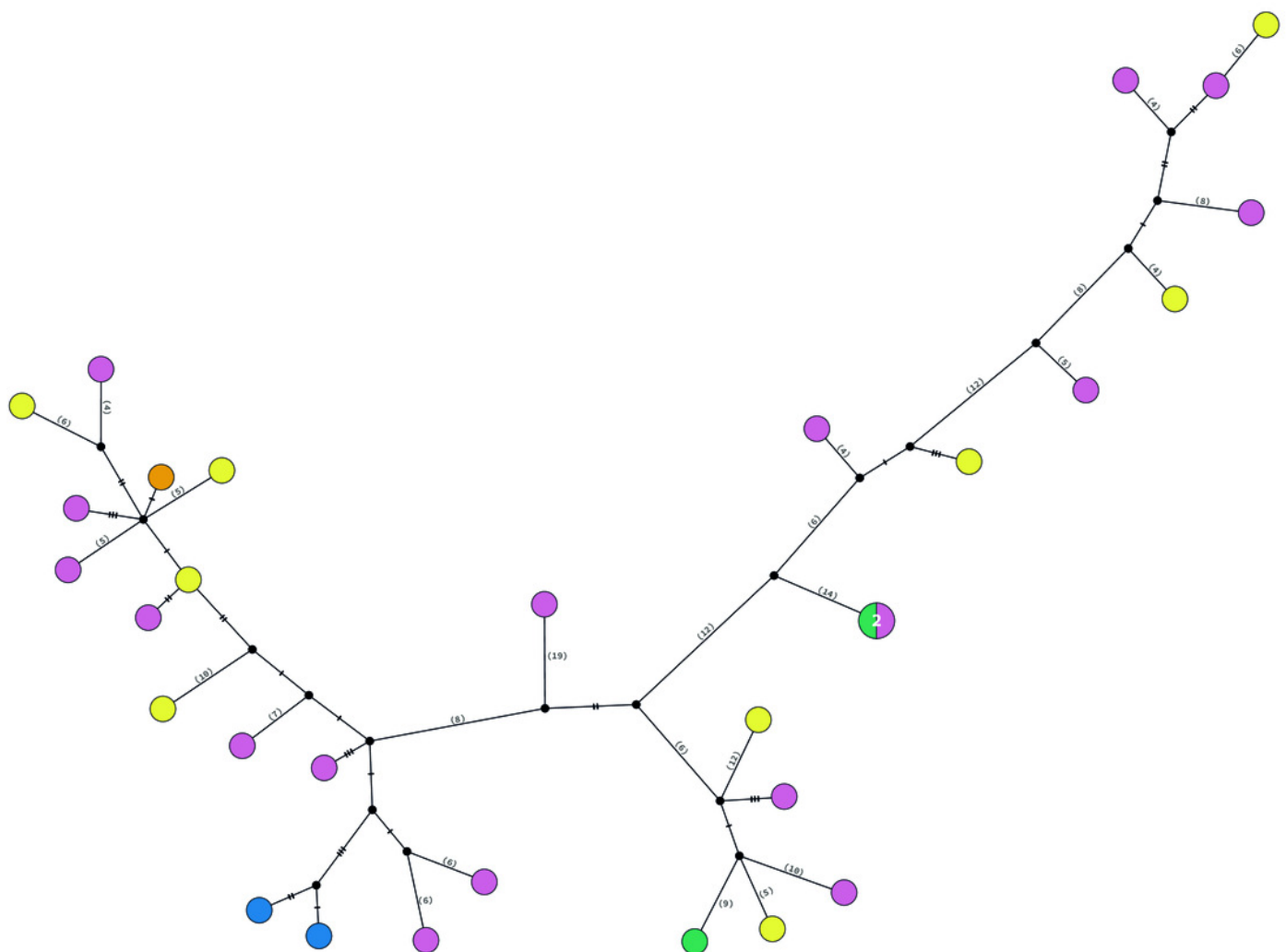
Figure 7

Geometric Morphometrics - Dorsal Arm Plate

Dorsal arm plate geometric morphometrics. Scatterplots showing shape variation along principal component axes. Clade 1A (green). Clade 1B (orange). Clade 2 (blue). Clade 3 (pink). Thin-plate spline deformation grids accompany each PC axis to show the specimens' shape at their positive and negative ends; the arm plate consensus shape is gray. The bar graph depicts the percentage of variance explained by PC axes.
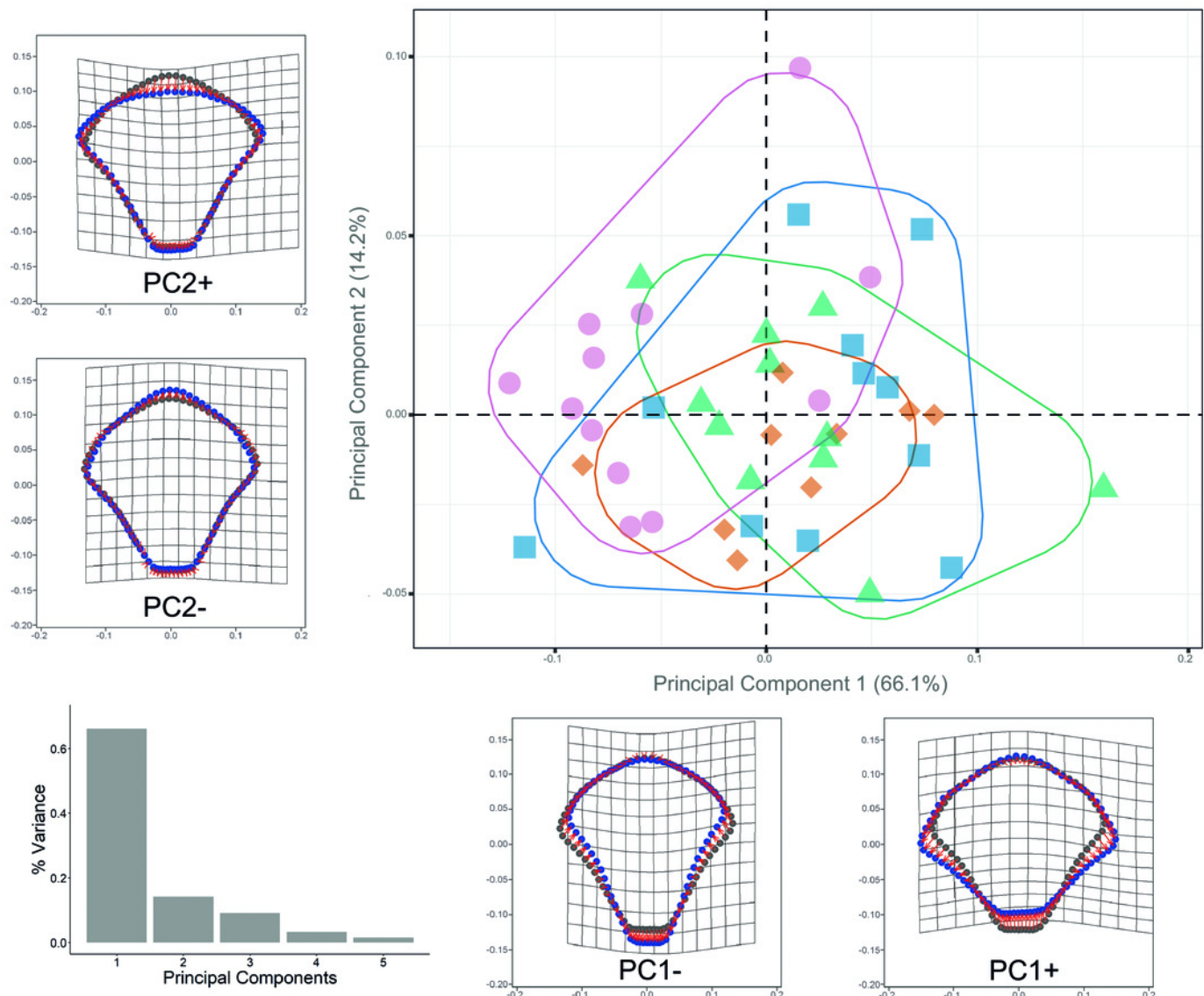
Figure 8

Geometric Morphometrics - Ventral Arm Plate

Ventral arm plate geometric morphometrics. Scatterplots showing shape variation along principal component axes. Clade 1A (green). Clade 1B (orange). Clade 2 (blue). Clade 3 (pink). Thin-plate spline deformation grids accompany each PC axis to show the specimens' shape at their positive and negative ends; the arm plate consensus shape is gray. The bar graph depicts the percentage of variance explained by PC axes.
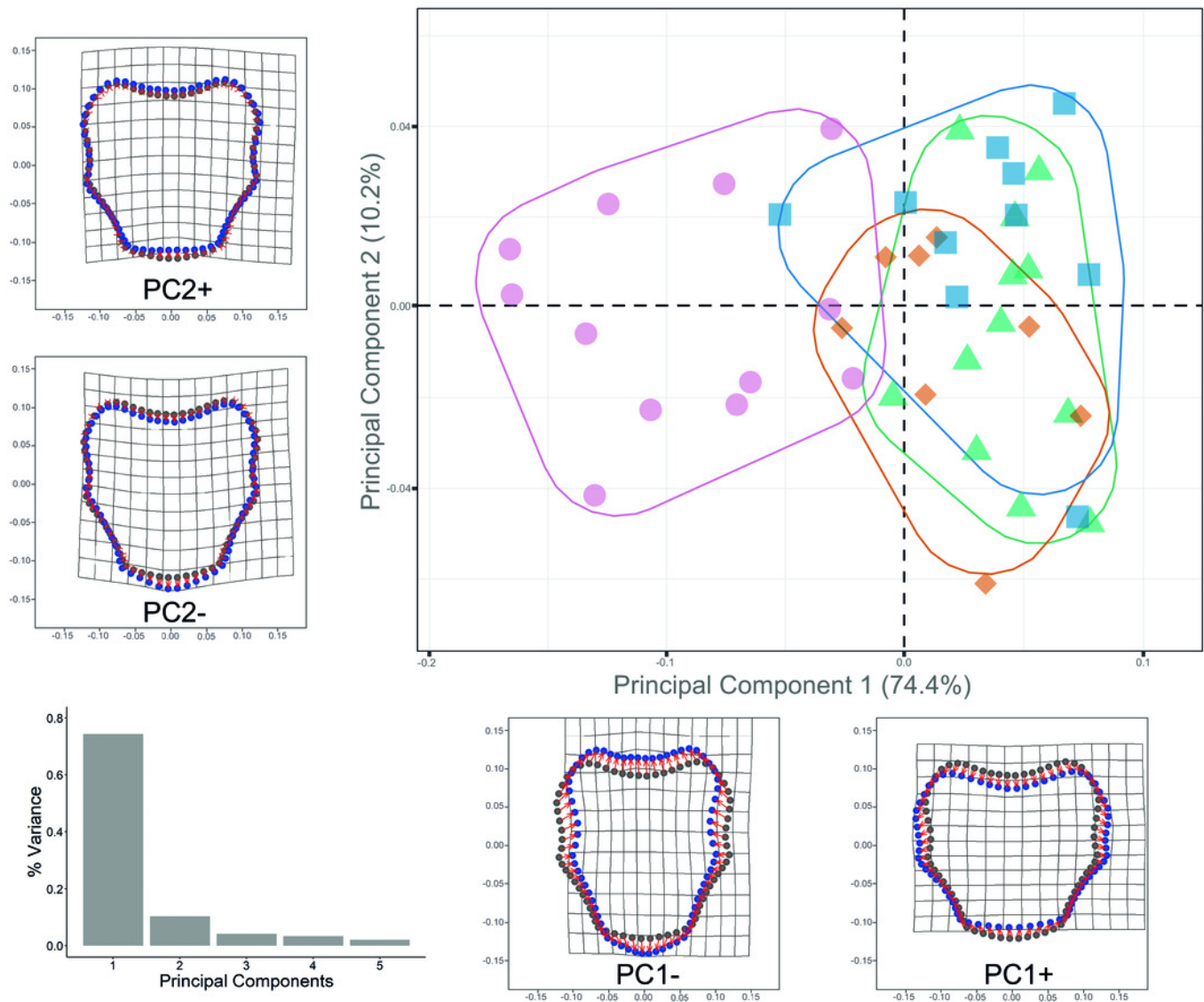
Figure 9

Molecular and morphological species delimitation

Species delimitation for *Ophiothrix angulata* clades based on molecular, morphological, and integrative approaches. Clade 1A (UF7632), Clade 1B (UF11608), Clade 2A (UF10248), and Clade 3 (UF10250). COI phylogeny on the left, representative specimen based on DAP and VAP consensus shape of major clades in the middle, species delineations on the right. Delineated species are represented by separate colors. iBPP results are based on a) COI and arm color information (Seq+COL) and b) COI and geometric morphometric data (Seq+GM). ND: no data. Photo credit: Invertebrate Zoology Collection, Florida Museum of Natural History, University of Florida.
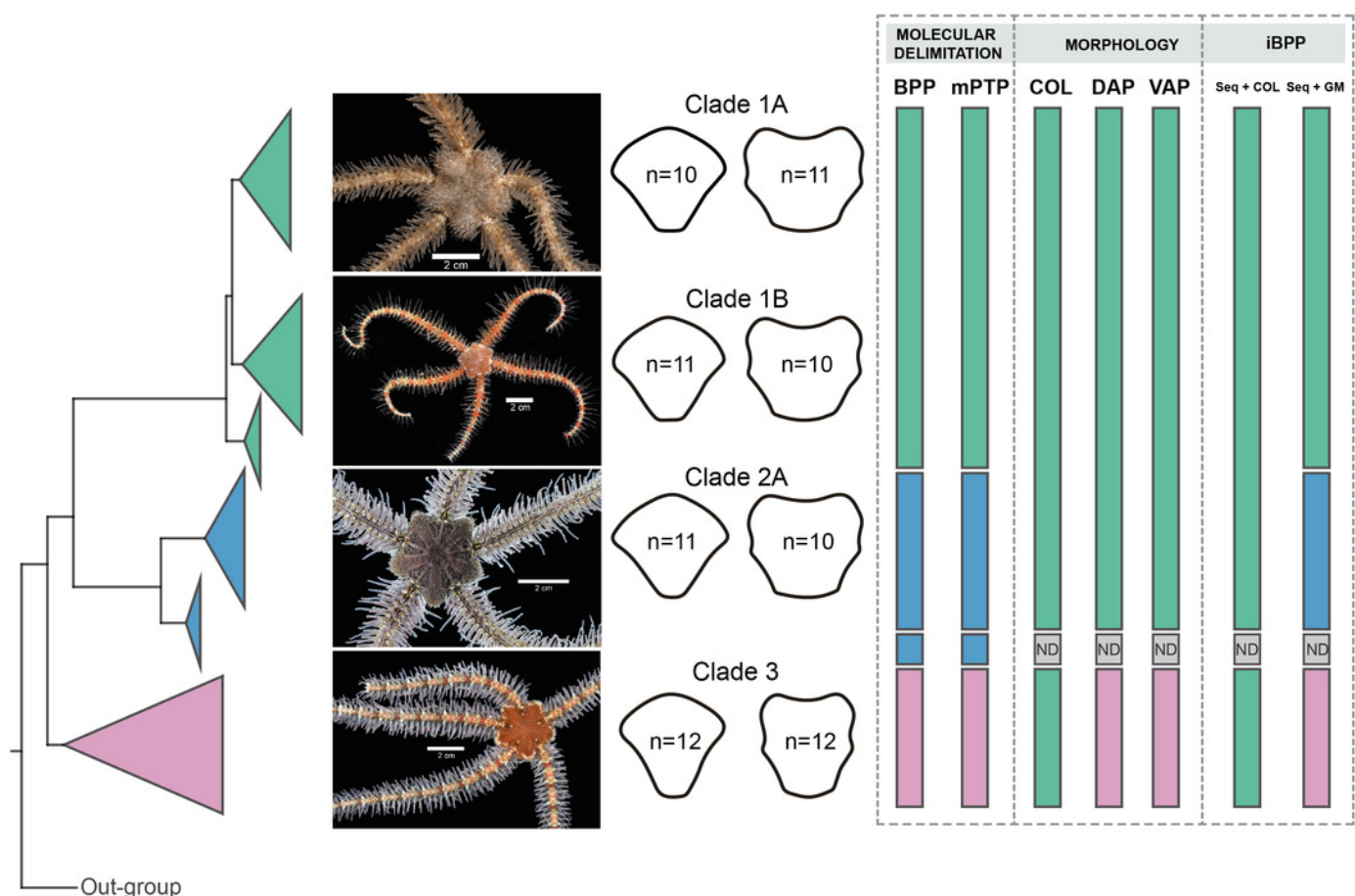
Genetic distances *Ophiothrix*

Genetic distances (± standard error) between recovered clades of *O. angulata* based on a Kimura 2-Parameters model for COI. Inter-specific distance values are presented below the diagonal. Numbers along the diagonal in bold and brackets represent intra-specific variation. Genetic distances were compared with the congeneric species *Ophiothrix lineata* and *O. suensoni* distributed in the Caribbean and Gulf of Mexico; *Ophiothrix cimar* distributed in the Caribbean and *Ophiactis savignyi* (outgroup).

COI	Clade 1	Clade 2	Clade 3	*O. cimar*	*O. lineata*	*O. suensoni*	*O. savignyi*
Clade 1	**[0.032 ± 0.004]**						
Clade 2	0.170 ± 0.019	**[0.007 ± 0.001]**					
Clade 3	0.279 ± 0.028	0.264 ± 0.026	**[0.053 ± 0.006]**				
O. cimar	0.316 ± 0.032	0.310 ± 0.033	0.278 ± 0.028	–			
O. lineata	0.276 ± 0.028	0.253 ± 0.027	0.254 ± 0.026	0.133 ± 0.016	–		
O. suensoni	0.304 ± 0.030	0.278 ± 0.029	0.274 ± 0.028	0.243 ± 0.027	0.264 ± 0.028	–	
O. savignyi	0.323 ± 0.032	0.302 ± 0.031	0.319 ± 0.032	0.279 ± 0.030	0.263 ± 0.027	0.302 ± 0.032	–

Summary statistics and demographic analyses

Summary statistics and demographic analyses for the largest clades of *O. angulata*, including N=number individuals, Number of haplotypes, *h*=haplotype diversity, *π*=nucleotide diversity ± standard deviation, SSD=Sum of squared differences in mismatch analysis, Mismatch distribution raggedness index (*r*), results of Fu's *Fs*. Clade 1C was not considered because its n=3.

Clades	N	Number of haplotypes	h	π	SSD		Raggedness r		Fu's Fs	
					SSD	p-value	r	p-value	Fs	p-value
Clade 1	76	74	0.999 ± 0.003	0.032 ± 0.001	0.023	0.129	0.005	0.320	-72.71	0.000
Clade 1A	44	43	0.998 ± 0.005	0.010 ± 0.001	0.004	0.143	0.018	0.156	-34.17	0.000
Clade 1B	29	29	1.000 ± 0.009	0.026 ± 0.002	0.013	0.187	0.007	0.889	-18.64	0.000
Clade 2	51	23	0.743 ± 0.068	0.007 ± 0.002	0.006	0.810	0.015	0.972	-11.73	0.000
Clade 3	31	30	0.998 ± 0.009	0.048 ± 0.003	0.004	0.914	0.009	0.574	-08.73	0.007